Journal of Solid State Chemistry 184 (2011) 2961–2965

Contents lists available at SciVerse ScienceDirect

Journal of Solid State Chemistry

journal homepage: www.elsevier.com/locate/jssc

# Topotactic synthesis of $Co_3O_4$ nanoboxes from $Co(OH)_2$ nanoflakes

Li Tian [a,b,*], Kelong Huang [b], Younian Liu [b], Suqin Liu [b]

[a] School of Chemistry and Chemical Engineering, Hunan University of Science and Technology, Xiangtan 411201, China
[b] School of Chemistry and Chemical Engineering, Central South University, Changsha 410083, China

ARTICLE INFO

*Article history:*
Received 27 May 2011
Received in revised form
28 July 2011
Accepted 22 August 2011
Available online 1 September 2011

*Keywords:*
Solvothermal synthesis
Crystal morphology
Topotactic growth

ABSTRACT

Hollow nanocubes of spinel $Co_3O_4$ with the dimension of 20 nm were successfully prepared via a facile and reproducible solvothermal route. The structure and morphology of $Co_3O_4$ nanoboxes were characterized by powder X-ray diffraction (XRD), scanning electron microscopy (SEM) and high-resolution transmission electron microscope (HRTEM) techniques. And a possible growth mechanism of $Co_3O_4$ nanoboxes were suggested that solid $Co_3O_4$ nanocubes nucleate in-situ and grow epitaxially from hexagonal β-$Co(OH)_2$ precursors with the structural matching relationship of [0 0 1] β-$Co(OH)_2$//[1 1 1] $Co_3O_4$, and then solid $Co_3O_4$ nanocubes gradually hollow and convert to single-crystal nanoboxes owing to Ostwald ripening.



## 1. Introduction

$Co_3O_4$ is an important magnetic p-type semiconductor with the normal spinel structure represented as $AB_2O_4$. In the past few years, $Co_3O_4$ has received considerable attention due to its much intriguing magnetic, optical, electronic, and electrochemical properties [1–35] and broad practical applications in heterogeneous catalysts, anode materials in Li-ion rechargeable batteries, solar energy absorbers, solid-state sensors, electrochromic devices, and magnetic materials [1–13]. Nano-sized $Co_3O_4$ with hollow structure is especially attractive for optimizing properties and enhancing performances [14–17].

It is well known that the intrinsic properties and practical applications of inorganic materials depend on their morphologies and crystallinity, such as crystallite sizes, shapes and orientations, which are related to the preparation methodology [18,19]. In order to develop new functional materials with enhanced performance, many researchers endeavored to investigate the rational design and controllable preparation of nanostructured functional materials with specific size, phase, and morphology. For $Co_3O_4$, a growing effort has been made to optimize the synthesis of nanostructural materials and strengthen their applications. To date, many synthesis approaches have been achieved, such as thermal decomposition, sol–gel, spray pyrolysis and microemulsion [20–26]. And a variety of $Co_3O_4$ crystals with different nanostructures have been obtained [7,27].

In this paper, we report the fabrication of single-crystal $Co_3O_4$ nanoboxes with the diameter of 20 nm and the wall-thickness of 5 nm by one-pot solvothermal process. The successful preparation of spinel $Co_3O_4$ nanoboxes is attributed to the topotactic relationship of [0 0 1] β-$Co(OH)_2$//[1 1 1] $Co_3O_4$ in crystallography. The topotactic chemical synthesis maybe provides a rational and versatile method to prepare nanostructured metal oxides.

## 2. Experimental section

### 2.1. Materials and physical techniques

All reagents and solvents for the synthesis and analysis were commercially available and used as-received. The as-synthesized

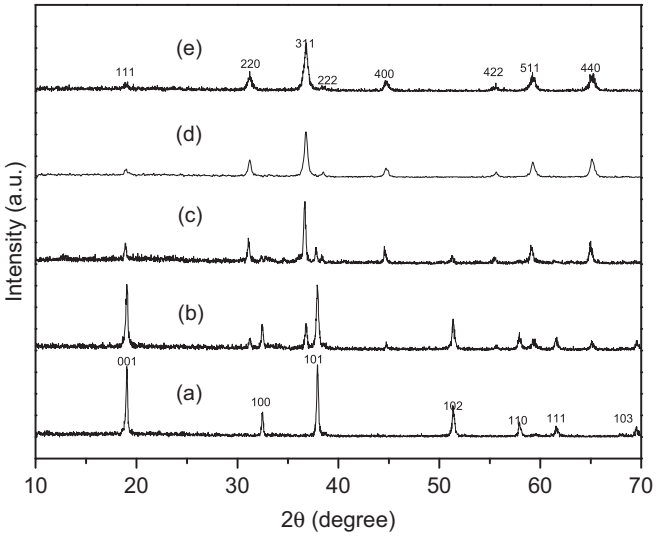


**Fig. 1.** Powder XRD patterns of the products prepared after a facile autoclaving process at 180 °C for 3.0 h (a), 6.0 h (b), 12 h (c), 18 h (d) and 24 h (e).

* Corresponding author at: School of Chemistry and Chemical Engineering, Hunan University of Science and Technology, Xiangtan 411201, China.
Fax: 86 73158290287.
*E-mail address:* ltian@hnust.edu.cn (L. Tian).

0022-4596/$ - see front matter © 2011 Elsevier Inc. All rights reserved.
doi:10.1016/j.jssc.2011.08.026

samples were characterized by powder X-ray diffraction (XRD), scanning electron microscopy (SEM), transmission electron microscopy (TEM), and high-resolution TEM (HRTEM). Powder XRD patterns were collected on a Rigaku D/MAX 2200 VPC diffractometer using a Cu $K\alpha$ radiation ($\lambda=0.15045$ nm) and a graphite monochromator operating at 40 kV and 30 mA with a $2\theta$ scanning rate of $10^{\circ}\ min^{-1}$. SEM images were taken with FEI Quanta 400 thermal FE environment scanning electron microscope. Dried samples for SEM were placed on glass-slide surfaces and then sputter-coated with platinum. TEM and selected-area electron diffraction (SAED) analyses were performed on a JEOL-2010 high-resolution transmission electron microscope operated at an accelerating voltage of 200 kV. TEM samples were prepared by dispersing the powders on carbon film supported on copper grids.

### 2.2. Synthesis of $Co_3O_4$ nanoboxes

In a typical synthesis, 0.374 g (1.5 mmol) of $Co(OAc)_2\cdot 4\,H_2O$ were dissolved in 4.0 mL of distilled water under vigorously magnetic stirring, followed by adding 4.0 mL of *n*-butanol and 12 mL of ammonia. The resulting solution was sealed in a 30-ml teflon-lined stainless steel autoclave and transferred into an electric oven at 180 °C for a period of time. When the reaction was completed, the autoclave was taken out and then naturally cooled down to room temperature. The dark product was separated by centrifugation and thoroughly rinsed with ethanol and distilled water to remove all residual contaminants, then dried in a desiccator at ambient temperature.

## 3. Results and discussion

### 3.1. XRD characterizations of $Co_3O_4$ nanoboxes

The phases of the products synthesized typically at 180 C were identified by XRD characterization. Fig. 1 shows the powder XRD patterns of the products obtained after different reaction times. The product after 3-h reaction is proved to be hexagonal β-$Co(OH)_2$ with brucite-like structure (JCPDS No. 30-0443, $a=b=0.3183$ nm,

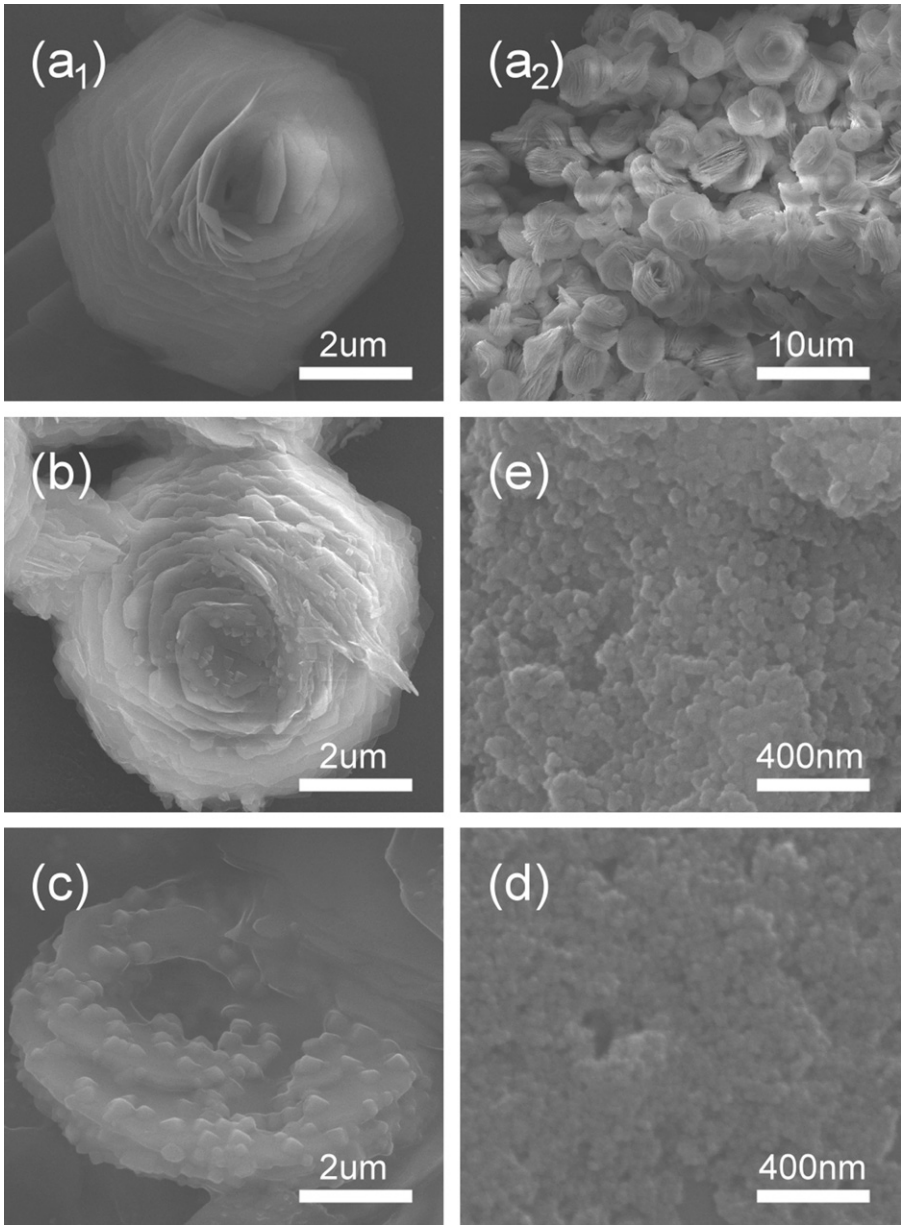


**Fig. 2.** FESEM images of the products prepared at 180 °C for 3.0 h ($a_1$; $a_2$), 6.0 h (b), 12 h (c), 18 h (d) and 24 h (e).

$c=0.4652$ nm), as shown in Fig. 1a. After 6.0 and 12 h, the products are mixtures of hexagonal β-$Co(OH)_2$ and cubic spinel $Co_3O_4$ (JCPDS No. 43-1003, $a=b=c=0.8084$ nm), as shown in Fig. 1b and c. And pure spinel phase is formed after 18- and 24-h reaction (Fig. 1d and e). The results indicate that there is a gradual replacement of the brucite-like cobalt hydroxide by spinel cobalt oxide during autoclaving aging.

### 3.2. SEM characterizations of $Co_3O_4$ nanoboxes

Fig. 2 shows SEM images of the products obtained after a facile autoclaving process at 180 °C for different hydrothermal times. The sole solid product after 3.0-h reaction is hexagonal β-$Co(OH)_2$. The β-$Co(OH)_2$ crystals were grown in flower-like morphology and composed of numerous hexagonal nanoflakes packed in a spiral way, as shown in Fig. 2$a_1$ and $a_2$. After 6.0-h reaction, the solid spinel nanocrystals were grown orientedly on the surface of the hexagonal brucite β-$Co(OH)_2$ nanoflakes. After 12-h reaction, more and more spinel nanocubes were formed in accordance with the powder XRD result (Fig. 1c), while β-$Co(OH)_2$ nanoflakes tended to deteriorate and gradually disappeared (Fig. 2c). After continuing reaction to 18 h, phase-pure and well-crystalline spinel nanocubes (Fig. 1d and Fig. 2d) were obtained. A few $Co_3O_4$ nanocubes with tiny hollow interiors became visible by TEM observation, as shown in subsequent Fig. 3e. Aging to 24 h, the hollow cubes with larger cavities were obtained (Fig. 3f and Fig. 4). The nanobox structures are important owing to their promising applications in many fields, such as in nanosized reactors, photonic devices, robust catalysts, controllable molecule-releasing capsules, ionic interalation, surface functionalization, active-materials encapsulation, drug delivery, and so on.

### 3.3. TEM characterizations of $Co_3O_4$ nanoboxes

Fig. 3 shows TEM images of the products prepared after the solvothermal reaction at 180 °C for 6.0, 12 and 24 h. The TEM image in Fig. 3a was taken from the top view of a β-$Co(OH)_2$

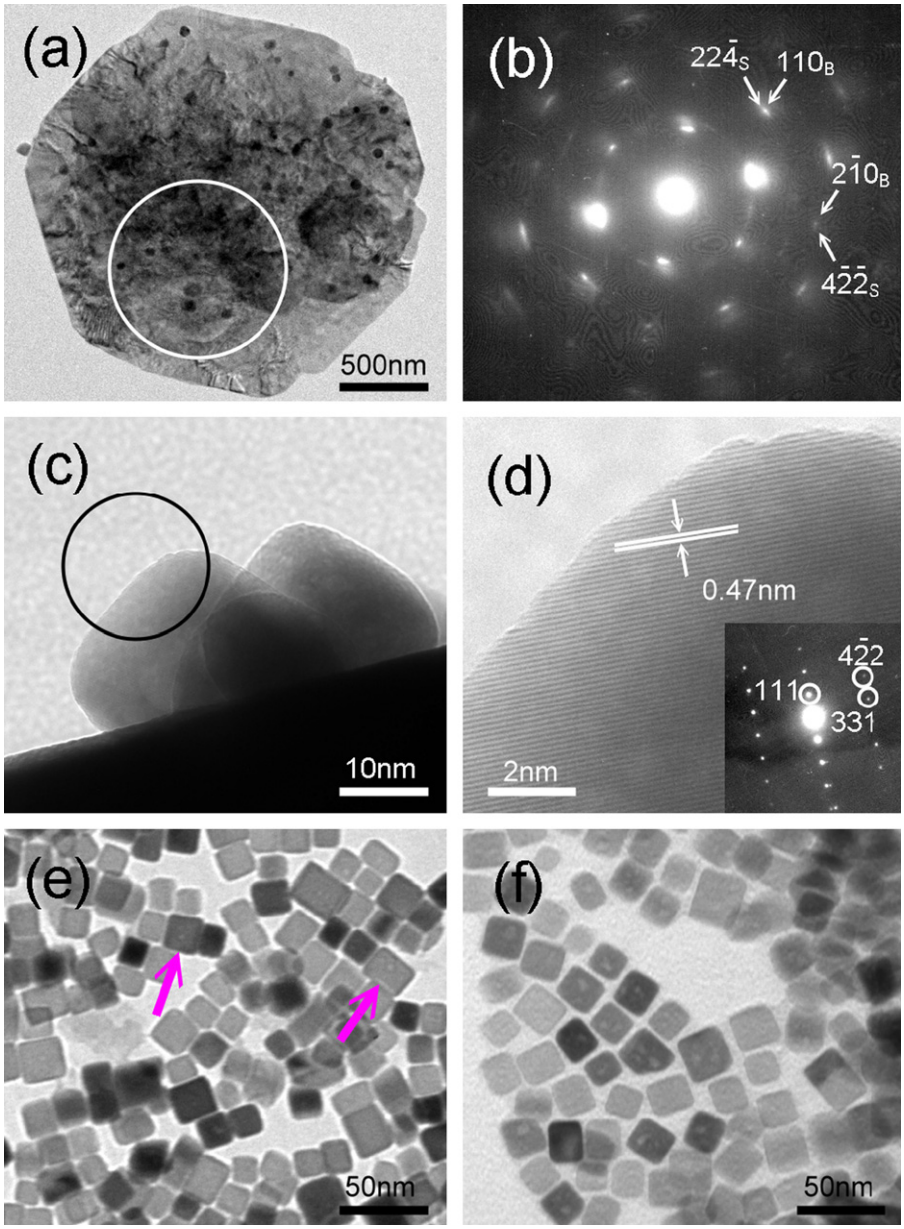


**Fig. 3.** TEM image taken from the top view of β-$Co(OH)_2$ nanoflake prepared at 180 °C for 6.0 h (a), the selected area electron diffraction (SAED) pattern obtained from the white circle in Fig. 3a (b), TEM micrograph of a hexagonal β-$Co(OH)_2$ plate with dotted nanocrystals viewed from the side of the plate (c), HRTEM image and SEAD pattern(inset) of the nanocrystal marked by the black cycle in Fig. 3c (d), TEM micrographs of $Co_3O_4$ nanocubes synthesized at 180 °C for 18 h (e) and 24 h (f).

nanoflake, showing that some nanoparticles came out from the hexagonal β-$Co(OH)_2$ nanoflake after 6-h reaction. The SAED pattern (Fig. 3b) contains two sets of diffraction spots: one from hexagonal β-$Co(OH)_2$ phase (marked by subscript B), and the other from spinel $Co_3O_4$ phase (marked by subscript S). And the SAED pattern indicates that the [1 1 1] axes of spinel nanocrystals are parallel to the [0 0 1] axis of hexagonal β-$Co(OH)_2$, which demonstrates that spinel-structured $Co_3O_4$ nanocubes have a possible topotactic nucleation and crystallization with their [1 1 1] directions inheriting the [0 0 1] directions of brucite-like structured β-$Co(OH)_2$ nanoflakes. The TEM micrographs in Fig. 3c is taken from side view to show the arrays of $Co_3O_4$ nanocubes grown on the β-$Co(OH)_2$ plates. The relevant HRTEM image of the area marked by a black cycle in Fig. 3c indicates a highly crystalline character of a considerably distinct lattice spacing of 0.47 nm corresponding to the value of the (1 1 1) planes of spinel $Co_3O_4$. The SAED pattern inserted in Fig. 3d obviously supports its single-crystalline nature and oriented growth along [1 1 1] direction of spinel-structured $Co_3O_4$ or [0 0 1] direction of brucite-like structured β-$Co(OH)_2$.

With the reaction time increasing to 12 h, pure-phase $Co_3O_4$ could be obtained. As shown in Fig. 3e, the crystals with the cube geometry have a mean edge length of ca. 20 nm. Meanwhile, there is a little cavity occurred in some cubes as the arrowhead denoted. When the hydrothermal time prolonged to 24 h, $Co_3O_4$ nanocubes with uniformed morphology were obtained. The remarkable contrast between the nanocube edges and centers observed in bright field TEM image (Fig. 3f and Fig. 4) indicates the hollow nature of the $Co_3O_4$ nanocubes, which is attributed to Ostwald ripening in a solid-solution-solid process. At the preliminary nucleation period of the $Co_3O_4$ nanocubes, a number of solid crystal nuclei with poor crystallography and small dimension came into being in solution owing to the kinetic advantage. The dimension difference of the forming crystallites, then inevitably leads to the change of concentrations of solutes across the solution. Those crystals with smaller size and nanocrystallites located in the central part of the crystal particles were believed to dissolve continuously and be smaller due to their higher thermodynamic solubility, and would be relocated and evacuated finally, whilst the larger ones are essentially immobile. The uniformity of this concentration gradient will eventually eliminate crystals of smaller sizes [35]. As a result, the interior space was created through the dissolving and regrowing of nanocrystallites in the central part of the crystal particles. Ultimately, hollow $Co_3O_4$ nanocubes with a wall thickness of ca. 5 nm were received.

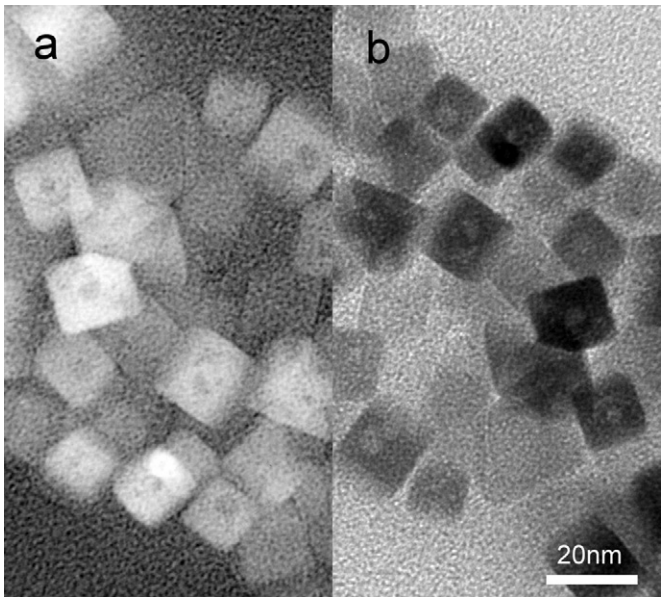


**Fig. 4.** Low-magnification dark-field (a) and bright-field (b) TEM images of $Co_3O_4$ nanocubes synthesized at 180 °C for 24 h.

### 3.4. Grown mechanism of $Co_3O_4$ nanoboxes

Based on the detailed time-dependent crystallization study, the formation mechanism of spinel $Co_3O_4$ nanoboxes can be expressed as a three-step process. (1) At the initial reaction stage, $Co^{2+}$ ions in the mixed solution react with $OH^-$ ions to form β-$Co(OH)_2$ nanoflake precursors. (2) Spinel nanoparticles nucleate orientively in situ on hexagonal β-$Co(OH)_2$ nanoplates and grow epitaxially to form $Co_3O_4$ nanocubes due to a topotactic transformation in crystallography. (3) Spinel $Co_3O_4$ nanocubes hollow gradually and transform to nanoboxes owing to Oswald ripening. The formation of $Co_3O_4$ nanocubes and the hollowing process could be schematically illustrated in Fig. 5.

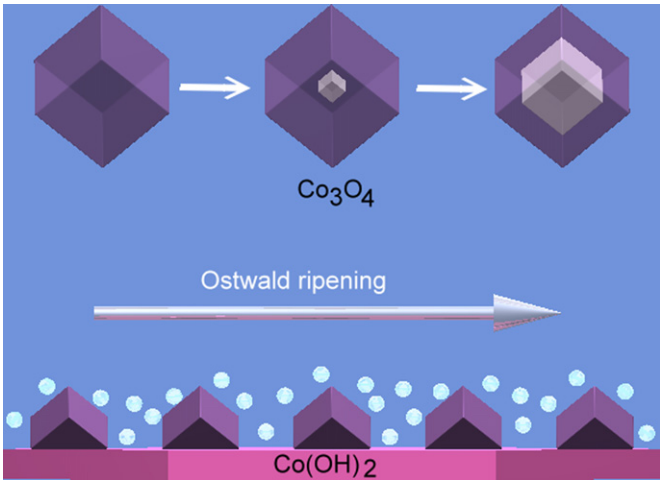


**Fig. 5.** Schematic illustration of the formation of $Co_3O_4$ nanocubes and the hollowing process.

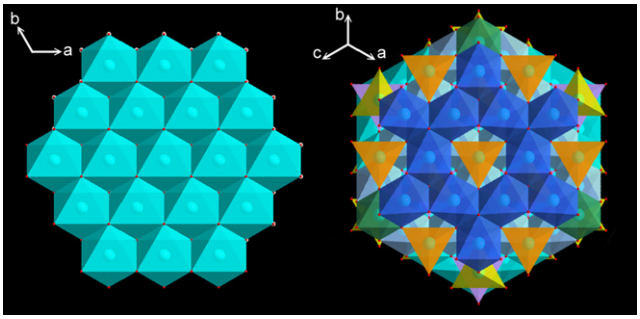


β-$Co(OH)_2$: [001] $Co_3O_4$:[111]

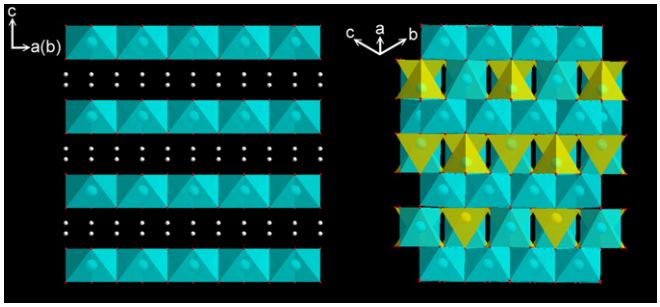


β-$Co(OH)_2$:[$0\bar{1}1$] $Co_3O_4$:[$2\bar{1}\bar{1}$]

**Fig. 6.** The structural match relationship between β-$Co(OH)_2$ and $Co_3O_4$ along and normal to their 〈0 0 1〉 and 〈1 1 1〉 directions. Different colored polyhedra indicate different coordinates along the normal of the page.

In fact, the successfully preparation of spinel $Co_3O_4$ nanoboxes is attributed to the close 3D structural matching between spinel $Co_3O_4$ and hexagonal β-$Co(OH)_2$. The structural matching relationship between the two phases of spinel $Co_3O_4$ and hexagonal β-$Co(OH)_2$ is shown in Fig. 6. Topotactic nucleation and grow epitaxially of spinel $Co_3O_4$ nanoparticles on β-$Co(OH)_2$ nanoplates take place with a preference for the specific $\langle 1\,1\,1 \rangle$ axes of spinel $Co_3O_4$ parallel to the $\langle 0\,0\,1 \rangle$ axis of β-$Co(OH)_2$ nanoplates, that is, $[1\,1\,1]_S//[0\,0\,1]_B$.

## 4. Conclusion

Monodispersed $Co_3O_4$ nanocubes have been synthesized by one-pot solvothermal method. $Co_3O_4$ nanocubes have hollow interior with edge lengths of about 20 nm and wall thicknesses of ca. 5 nm. The time-dependent experimental results indicate that $Co_3O_4$ nanoboxes were formed by the topotactic chemical transformation from β-$Co(OH)_2$ nanoplate precursors. The proposed growth mechanism of $Co_3O_4$ nanoboxes was studied in detail and it suggested that the $Co_3O_4$ nanocubes were formed due to the structural matching relationship of [0 0 1] β-$Co(OH)_2$//[1 1 1] $Co_3O_4$ and then hollowed owing to Oswald ripening. The topotactic synthesis may provide a rational and universal method to prepare nanostructured oxides.

## Acknowledgment

This work is supported financially by China Postdoctoral Science Foundation Project (No. 20100480947, No. 201104510), Postdoctoral Science Foundation of Central South University of China (No. 1332–74341015511), Doctor start-up research fund of Hunan University of Science and Technology (No. E51079), Education and Teaching fund of Hunan University of Science and Technology (No. G30953). L. Tian is grateful to Prof. M. M. Wu at Sun Yat-sen University in China for helpful direction.

## References

[1] Z.G. Guo, W.M. Liu, Appl. Phys. Lett. 90 (2007) 193108–193111.
[2] J. Li, S.B. Tang, L. Lu, H.C. Zeng, J. Am. Chem. Soc. 129 (2007) 9401–9402.
[3] B.X. Li, Y. Xie, C.Z. Wu, Z.Q. Li, J. Zhang, Mater. Chem. Phys. 99 (2006) 479–486.
[4] U. Kumar, A. Shete, A.S. Harle, O. Kasyutich, W. Schwarzacher, A. Pundle, P. Poddar, Chem. Mater. 20 (2008) 1484–1491.
[5] M.J. Benitez, O. Petracic, E.L. Salabas, F. Radu, H. Tuysuz, F. Schuth, H. Zabel, Phys. Rev. Lett. 101 (2008) 7026–7030.
[6] L. Cao, M. Lu, H.L. Li, J. Electrochem. Soc. 152 (2005) A871–875.
[7] E. Hosono, S. Fujihara, I. Honma, H.S. Zhou, J. Mater. Chem. 15 (2005) 1938–1945.
[8] A.M. Cao, J.S. Hu, H.P. Liang, W.G. Song, L.J. Wan, X.L. He, X.G. Gao, S.H. Xia, J. Phys. Chem. B 110 (2006) 15858–15863.
[9] Z. Dong, Y.Y. Xu, X.J. Zhang, W.T. Jin, P. Kashkarov, H. Zhang, Solid State Commun. 149 (2009) 648–651.
[10] C.Y. Ma, Z. Mu, J.J. Li, Y.G. Jin, J. Cheng, G.Q. Lu, Z.P. Hao, S.Z. Qiao, J. Am. Chem. Soc. 132 (2010) 2608–2613.
[11] B. Varghese, Y.S. Zhang, L. Dai, V.B.C. Tan, C.T. Lim, C.H. Sow, NanoLett 8 (2008) 3226–3232.
[12] L.H. Hu, Q. Peng, Y.D. Li, J. Am. Chem. Soc. 130 (2008) 16136–16137.
[13] Y.G. Li, B. Tan, Y.Y. Wu, Nano Lett. 8 (2008) 265–270.
[14] K.T. Nam, D.W. Kim, P.J. Yoo, C.Y. Chiang, N. Meethong, P.T. Hammond, Y.M. Chiang, A.M. Belcher, Science 312 (2006) 885–888.
[15] B. Varghese, T.C. Hoong, Z. Yanwu, M.V. Reddy, B.V.R. Chowdari, A.T.S. Wee, T.B.C. Vincent, C.T. Lim, C.H. Sow, Adv. Funct. Mater. 17 (2007) 1932–1939.
[16] Y.G. Li, B. Tan, Y.Y. Wu, Nano Lett. 8 (2008) 265–270.
[17] L. Tian, H.L. Zou, J.X. Fu, X.F. Yang, Y. Wang, H.L. Guo, M.M. Wu, Adv. Funct. Mater. 20 (2010) 617–623.
[18] L. He, C.P. Chen, N. Wang, W. Zhou, L. Guo, J. Appl. Phys. 102 (2007) 103911.
[19] J. Feng, H.C. Zeng, Chem. Mater. 15 (2003) 2829–2835.
[20] Y.S. Ding, L.P. Xu, C.H. Chen, X.F. Shen, S.L. Suib, J. Phys. Chem. C 112 (2008) 8177–8183.
[21] Y.L. Hou, H. Kondoh, M. Shimojo, K. Kogure, T. Ohta, J. Phys. Chem. B 109 (2005) 19094–19098.
[22] J.S. Li, B. Tang, L. Lu, H.C. Zeng, J. Am. Chem. Soc. 129 (2007) 9401–9409.
[23] X.M. Ni, J.M. Song, D.G. Li, Y.F. Zhang, F.G. Zheng, Chem. Lett. 36 (2007) 146–147.
[24] T. He, D.R. Chen, X.L. Jiao, Y.L. Wang, Adv. Mater. 18 (2006) 1078–1082.
[25] L.H. Zhuo, J.C. Ge, L.H. Cao, B. Tang, Cryst. Growth Des. 9 (2009) 1–6.
[26] K.B. Klepper, O. Nilsen, H. Fjellvag, J. Cryst. Growth 307 (2007) 457–465.
[27] J. Yang, H.W. Liu, W.N. Martens, R. L. J., Phys. Chem. C 114 (2010) 111–119.
[28] X.H. Liu, G.Z. Qiu, X.G. Li, Nanotechnology 16 (2005) 3035–3040.
[29] R.M. Wang, C.M. Liu, H.Z. Zhang, C.P. Chen, L. Guo, H.B. Xu, S.H. Yang, Appl. Phys. Lett. 85 (2004) 2080–2082.
[30] Y.G. Li, B. Tan, Y.Y. Wu, J. Am. Chem. Soc. 128 (2006) 14258–14259.
[31] F. Kurtulus, H. Guler, Inorg. Mater. 41 (2005) 483–485.
[32] F. Cheng, Z. Tao, J. Liang, J. Chen, Chem. Mater. 20 (2008) 667–681.
[33] X.W. Lou, D. Deng, J.Y. Lee, J. Feng, L.A. Archer, Adv. Mater. 20 (2008) 258–262.
[34] Y. Liu, C.H. Mi, L.H. Su, X.G. Zhang, Electrochim. Acta 53 (2008) 2507–2513.
[35] H.C. Zeng, Curr. Nanosci. 3 (2007) 177–181.